

Colorectal cancer survival prediction using deep distribution based multiple-instance learning

Xingyu Li¹, Jitendra Jonnagaddala^{2*}, Min Cen¹, Hong Zhang^{1*}, Xu Steven Xu^{3*}

¹ Department of Statistics and Finance, School of Management, University of Science and Technology of China, Anhui, P.R.China

² School of Population Health, UNSW Sydney, NSW, Australia.

³ Clinical Pharmacology and Quantitative Science, Genmab Inc., Princeton, New Jersey, USA.

* Corresponding author

Abstract:

Several deep learning algorithms have been developed to predict survival of cancer patients using whole slide images (WSIs). However, identification of image phenotypes within the WSIs that are relevant to patient survival and disease progression is difficult for both clinicians, and deep learning algorithms. Most deep learning based Multiple Instance Learning (MIL) algorithms for survival prediction use either top instances (e.g., maxpooling) or top/bottom instances (e.g., MesoNet) to identify image phenotypes. In this study, we hypothesize that wholistic information of the distribution of the patch scores within a WSI can predict the cancer survival better. We developed a distribution based multiple-instance survival learning algorithm (DeepDisMISL) to validate this hypothesis. We designed and executed experiments using two large international colorectal cancer WSIs datasets - MCO CRC and TCGA COAD-READ. Our results suggest that the more information about the distribution of the patch scores for a WSI, the better is the prediction performance. Including multiple neighborhood instances around each selected distribution location (e.g., percentiles)

could further improve the prediction. DeepDisMISL demonstrated superior predictive ability compared to other recently published, state-of-the-art algorithms. Furthermore, our algorithm is interpretable and could assist in understanding the relationship between cancer morphological phenotypes and patient's cancer survival risk. DeepDisMISL algorithm is available at <https://github.com/1996lixingyu1996/DeepDisMISL>

1 Introduction

Traditional risk stratification in cancer patients is usually based on cancer staging, grading, and, molecular and clinical characteristics[1-3]. Tumor grade based on cellular appearance has been shown to be a measure of prognosis and an indicator of how quickly a tumor is likely to grow and spread[4]. However, high inter-observer variability has been a major challenge [5]. Histopathology whole slide images (WSIs) are large with Giga pixels, it is extremely challenging to process on a General Processing Unit (GPU) at once. With the advances in the computer vision, deep learning algorithms using WSIs have been successfully applied to predicting patient outcomes such as, overall survival, progression free survival, time to metastasis, or tumor recurrence. Additionally, WSIs are also used to stratify patients according to their survival risk [6-8].

Different strategies have been proposed to enable processing WSIs on a GPU and predict patient outcomes based on image patches in the research area of deep-learning survival modeling using WSIs. Most often, WSIs are usually split into small image patches to train neural networks to predict an outcome. Due to the large number of image patches for each WSI that can vary from hundreds to thousands, and unavailability of patch-level labels, it is not feasible to directly build a prediction model at patch level. Multiple-instance learning (MIL) which is a form of weakly supervised learning where only coarse-grained labels are supplied can be used to predict outcomes at patient level [9]. For example, Zhu et al. and Wulczyn et al. randomly sampled patches from region of interests (ROIs) annotated by pathologists [7, 10]. Tissue Segmentation has been utilized to select relevant tissue type or

create new, higher-level features for survival prediction, such as percentage of different tissue types, ratio of the area of lymph node and tumor regions, hand-crafted features of intra-tumoral stroma [11-15]. Unsupervised clustering has also been used to select representative patches with similar features using [6, 7, 16, 17] .

Identification of WSI patches with the most predictive through MIL formulation is another strategy. Current evidence suggests that maximum scoring instances often carry the most predictive information for prediction. Therefore, large number of the studies adapted max-pooling (the maximum score of all instances) to aggregate the instance level information [18]. Recently, Durand et al. proposed an deep neural network multiple instance learning algorithm, WELDON, which selected and aggregated top and bottom instances (the highest and lowest scoring patches, respectively) for classification, which demonstrated improved performance compared to max-pooling and mean-pooling [19]. Courtiol et al. further modified the WELDON model and proposed CHOWDER to classify breast cancer based on whole slide images [18]. Furthermore, Courtiol et al. adjusted CHOWDER with a cox-loss function and proposed MesoNet for survival data [8], and demonstrated that both top and bottom instances can be used to more accurately in stratify the risk and predict the survival of malignant mesothelioma patients.

1.1 Contributions

1. Novel Probability Distribution based Patch Aggregation

Although Courtiol et al. showed that top and bottom patch scores from the WSI can provide accurate binary classification of breast cancer and prediction of survival for malignant mesothelioma, we hypothesize that probability distribution based information of the patch scores, instead of the extreme top or bottom instances can better predict the survival risk associated more accurately. In this study, we demonstrated that, by gradually adding additional patch scores at different percentiles (e.g., 1st, 5th, 25th, 75th, 95th, and 99th percentiles) to the top and bottom instances (i.e., min and max patch scores, respectively), the predictive performance of survival prediction in colorectal cancer can be improved drastically. Our experiments proved the concept that the more information about the distribution of the patch scores for a WSI, the better prediction performance for the instance-based MIL algorithms (Figure 2).

2. Systematic evaluation

We systematically validated our approach by comparing with six baseline algorithms: MesoNet [20], DeepAttnMISL [6], Meanpooling, Maxpooling (Top 1 instance), Maxpooling (Top 10 instance) and MeanFeaturePool. We applied 5-fold cross validation on a large Australian colorectal cancer dataset – MCO CRC [21, 22]. Additionally, an external validation was performed using the TCGA COAD-READ dataset [23]. The proposed DeepDisMISL demonstrated superior and robust predictive ability compared to all the baseline algorithms. Specifically, compared to MesoNet, DeepDisMISL provided 6.3% and 2.8% improvement of mean C-index in the 5-fold cross-validation and external validation, respectively. In addition, DeepDisMISL also outperformed the most recently published, state-of-the-art algorithm, DeepAttnMISL for the MCO dataset, i.e., the mean C-index of

DeepDisMISL was markedly higher than that of DeepAttnMISL (0.647 vs. 0.606) for the MCO dataset.

3. Interpretability

Our algorithm is highly interpretable as such revealed that for a given tumor tissue, there is positive relationship between risk and the tile scores, whereas for a normal muscle tissue, a negative relationship between risk and tile scores was observed. This suggests that our algorithm can help to reveal the relationship between morphological phenotypes and patients' risk.

2. Methods

2.1 Datasets

The analysis included two large-scale datasets. Hematoxylin and eosin (H&E) stained whole slide images (WSIs, 40x) were collected from both MCO and TCGA CRC studies. The MCO dataset was made available through the SREDH Consortium (www.sredhconsortium.org). The MCO dataset consisted of patients who underwent curative resection for colorectal cancer between 1994 to 2010 in New South Wales, Australia[21, 22]. The Cancer Genome Atlas (TCGA) public dataset included the TCGA-COAD and TCGA-READ datasets. The MCO dataset (v15Jan2021) was used to train the deep learning model while the TCGA dataset obtained in July 2020 was used for external validation. For patients with more than one WSI available, we randomly selected one slide for each patient. Images with annotation marks or blur were excluded. After exclusion, 1184 WSIs from 1184 patients MCO patients

were included in the analysis, whereas 529 WSIs from 529 patients were available from the TCGA database.

2.2 Preprocessing of WSIs

WSIs were first preprocessed to exclude the background area of each image where no tissue was present. OTSU algorithm was implemented to classify the image into two classes: the foreground (containing the matter) and background [24]. After removing the backgrounds, WSIs were cropped to non-overlapping, fixed-size tiles of images ($224 * 224$ pixels, 0.5mpp), which were then color normalized with Macenko's method. Depending on the size of the image, the number of tiles varied from a few hundred to 50,000 with a median of 12,047.

2.3 Feature extraction

We extracted features using a fine-tuned Xception model [25]. This neural network allowed us to obtain 256 relevant features from each tile. For each WSI (patient), a feature matrix with a dimension of n (number of tiles) \times 256 (features) was obtained. We randomly selected 12,000 tiles from the feature matrix of each patient. If the tile number per slide was smaller than 12,000, we would resample the feature matrix up to the size of 12,000.

2.4 DeepDisMISL

Figure 1 shows the proposed DeepDisMISL algorithm. We incorporated MIL before predicting on the unlabeled tiles. WSIs were considered the bags of MIL (each WSI can be considered as a bag, and patches of the WSI can be seen as instances), for which supervision was provided only for the bag at individual patient level (i.e., survival time \mathbf{t} and survival status δ for a patient), and the individual label of the instances contained in the bags (i.e., tiles)

were not available. Two convolution one-dimensional (1-D) layers with ReLU activation were used to aggregate all the local features of the same tile into a global feature and devised a score (the element in the vector of $12000 * 1$, each element can be seen as a score, Figure 1 and Table 2) for each tile. The scores at the selected percentiles (instances) of the global feature vector were the input features for the next prediction layer, which consisted of a two-layer multi-layer perceptron (MLP) classifier with two fully connected layers (128 and 64 neurons) and a ReLU activation for predicting survival risk with a cox loss function to deal with the censored survival data. The log likelihood function of the cox loss function used is equation 1 . Where O_i is the risk score, δ_i is the censoring variable ($\delta = 0$, death was not been observed). The neural network minimized the negative log partial likelihood function and produced maximum partial likelihood estimates.

$$L(O_i) = \sum_i \delta_i (-O_i - \log \sum_{j:t_j \geq t_i} \exp(O_j))$$

Equation 1: Log likelihood function of the cox loss function

We started with top/bottom instances (i.e., minimum, and maximum patch scores, or 0 and 100th percentile), and incrementally added additional instances at different percentiles to the top/bottom instances. In total, 7 different scenarios were investigated, i.e.,

(Scenario 1) [0, 100%],

(Scenario 2) [0, 0.1%, 99.9%, 100%],

(Scenario 3) [0, 0.1%, 1%, 99%, 99.9%, 100%],

(Scenario 4) [0, 0.1%, 1%, 5%, 95%, 99%, 99.9%, 100%],

(Scenario 5) [0, 0.1%, 1%, 5%, 10%, 90%, 95%, 99%, 99.9%, 100%],

(Scenario 6) [0, 0.1%, 1%, 5%, 10%, 25%, 75%, 90%, 95%, 99%, 99.9%, 100%], and

(Scenario 7) [0, 0.1%, 1%, 5%, 10%, 25%, 50%, 75%, 90%, 95%, 99%, 99.9%, 100%].

Zhu et al. showed that increasing number of top instances could improve the model performance. We also evaluated whether the number of neighborhood instances around each percentile has impact on the model predictive ability. In this experiment, we took the model with the most complete distribution (Scenario #7) and explored different number of neighborhood instances at each percentile (i.e., 1, 3, 5, and 7).

2.5 Baseline algorithms

We compared our algorithm with following different baseline algorithms (Figure 1): MesoNet [19], Meanpooling and Maxpooling (Top 1 and Top 10 instance) , MeanFeaturePool and DeepAttnMISL [6]. Similar to DeepDisMISL, MesoNet used two 1-D convolution layers to aggregate all local feature descriptors of a tile into a global feature vector. Then, the largest and smallest 10 scores from the global feature vector were selected as the features for the classifier in the prediction layer. Similarly, Meanpooling and Maxpooling (Top 1 instance) used the mean score and max score, respectively, from the global feature vector generated by 1-D convolution layers as the features for the classifier in the prediction layer. Maxpooling (Top 10 instance) used the largest 10 scores from the global feature vector as the features for the classifier in the prediction layer. For Meanpool (Lasso cox), the features values for all tiles (12, 000) from a feature matrix (12000 x 256) for each WSI was averaged to obtain an average feature vector (1 x 256) for each WSI or patient.

Lasso cox implemented in R package glmnet [26] was used to fit the survival data. The C-index values from a 5-fold cross validation were obtained from [13]. Both DeepAttnMISL [13] and our proposed DeepDisMISL used MCO dataset for cross validation, and the C-index values were compared directly. We further compared the performance of DeepDisMISL with the other baseline algorithms by examination of their ability for risk stratification. For each model, the median risk score in the training set was calculated and then applied as a threshold to stratify each patient into high-risk or low-risk group.

2.6 Annotation of WSI patches

To interpret the model, we annotated the patches near the different percentiles of the patch scores. Kather et al. developed a deep-learning classifier to classify CRC image tiles into eight tissue types: adipose tissue (ADI), background (BACK), debris (DEB), lymphocytes (LYM), mucus (MUC), smooth muscle (MUS), normal colon mucosa (NORM), cancer-associated stroma (STR), and colorectal adenocarcinoma epithelium (TUM).[27] We used pathologist annotated NCT-CRC-HE-100K and CRC-VAL-HE-7K image sets provided by Kather et al. to train and validate, respectively, a similar tissue-type classifier. We downloaded the Xception model from Keras and fine-tuned the model using the NCT-CRC-HE-100K set to develop the tissue-type classifier[25]. The overall accuracy of the tissue-type classification model was 99% based on training dataset, NCT-CRC-HE-100K and 94.4% based on the validation image set, CRC-VAL-HE-7K (Supplementary Figure 1). The tissue type of each image tile from the TCGA dataset was predicted using the fine-tuned Xception-based tissue-type classifier.

2.7 Evaluation

All models were trained using 5-fold cross validation on the MCO dataset. In each fold, 80% of the data were used for model training and 20% of the data were used for model validation. For training, we used Adam optimization with grid search strategy. The training process monitored the loss on the MCO validation dataset and was designed to stop if the loss increased goes increased much. We evaluated the model performances with concordance index (C-index) in the survival prediction task. The TCGA data served as the independent, external validation dataset.

3 Results

3.1 Evaluation of probability distribution-based patch selection

Figure 2a shows that, based on the 5-fold cross validation using the MCO dataset, there is an obvious trend where the more percentiles, the higher the C-index. With the top/bottom instances (See Figure 1 c), the average C-index was 0.611 (range: 0.58 – 0.630). Adding 2 more percentiles at 0.1% and 99.9% (Scenario #2) improved the average C-index to 0.62 (0.59 – 0.638). As expected, Scenario #7 with the most complete distribution information (0, 0.1%, 1%, 5%, 10%, 90%, 25%, 50%, 75%, 95%, 99%, 99.9%, 100%) produced the best predictive performance with an average C-index of 0.638 (0.626 – 0.66). The increasing trend in C-index suggests that the complete distribution of the patch scores carries richer information of the WSI than the only top and bottom instances (Figure 3).

Similarly, the external validation using an independent TCGA COAD-READ dataset demonstrated a similar trend (Figure 2b). In general, the models with more complete distribution provides higher C-index compared to those with less complete distribution (e.g., only the highest and lowest scoring patches. As expected, the external validation with independent dataset produced more heterogeneous results and lower C-index compared to the cross validation since the TCGA dataset does not completely resemble the MCO dataset. Nevertheless, the external validation with the TCGA dataset still preserved the overall trend where more complete distribution of the patch scores provided better predictive ability than the extreme top/bottom instances.

3.2 Multiple Neighborhood Instances vs. Single Instance at Each Percentile

Figure 3 clearly shows that multiple instances outperformed the single instance at each percentile. For the cross validation using the MCO dataset, the average C-index was improved from 0.640 to 0.645 when the number of instances at each percentile increased from 1 to 3 (Figure 3a). The average C-index increased to 0.647 with 5 neighborhood instances, and the improvement appears to level off with more neighborhood instances (i.e. 7). Similar pattern was observed with the independent TCGA dataset. The average C-index plateaued (0.580) when the number of instances at each percentile increased to 3. Therefore, consistent with Zhu et al's finding, multiple neighborhood instances at each percentile can improve the model performance. However, experiments may be needed to determine the optimal number of instances for different tasks and models.

3.3 Comparison with Baseline Algorithms

Our proposed DeepDistMISL demonstrated superior predictive ability compared to all the baseline algorithms (Figure 4). Compared to MesoNet, DeepDistMISL provided an additional 6.3% and 2.8% improvement of mean C-index in the 5-fold cross-validation and external validation, respectively. In addition, DeepDisMISL also outperformed the most recently published, state-of-the-art algorithm, DeepAttnMISL for the MCO dataset., The mean C-index of DeepDisMISL was markedly higher than that of DeepAttnMISL (0.647 vs. 0.606) for the MCO dataset. The superiority of the proposed DeepDistMISL in both cross validation and external validation indicates the robustness of this algorithm and highlights the importance of using complete distribution of patch scores in predicting models. Furthermore, Maxpooling (both top 1 and top 10 instances) had the worst performance compared to other approach in both cross validation and external validation. Similar to the finding in Courtiol et al , although meanfeaturepool provided better performance than MesoNet in cross validation, it seems less robust and had lower C-index in the external validation (Figure 4b) compared to MesoNet [8]. It is interesting to notice that the simple meanpooling approach had the second-best performance. Meanpooling outperformed all the other baseline approaches in the internal cross validation using the MCO dataset and maintained its performance in the external validation (i.e., provided similar C-index to MesoNet and outperformed other baseline algorithms). It should be mentioned that the results of DeepAttnMISL were obtained directly from the previous publication, and no external validation was conducted for DeepAttnMISL [6].

3.4 Risk stratification ability

Figure 5 shows that DeepDisMISL provided the best risk stratification for both MCO and TCGA populations. Among all the studied deep learning algorithms, the DeepDisMISL provide the best risk stratification and the most statistically significant separation of the survival curves between the high- and low-risk groups in both MCO and TCGA populations ($p < 0.0001$ in MCO and $p = 0.01$ in TCGA). That is, the DeepDisMISL identified high-risk subgroup presented significantly worse overall survival compared to the low-risk subgroup. MesoNet identified risk groups also showed apparent separation for survival, but with slightly larger p values ($p = 0.001$ in MCO and $p = 0.02$ in TCGA) compared to those based on DeepDisMISL. However, the other baseline algorithms (Meanpooling, Maxpooling with top 1 instance, maxpooling with top 10 instances, and MeanFeaturePool) only provided clear risk stratification in the MCO (training) dataset. In the TCGA (external validation) dataset, no statistically significant separation was observed.

3.5 Interpreting DeepDisMISL

Figure 7 shows the relationship between the risk and the percentiles of the tile scores. Every percentile appears correlated with risk, i.e., a positive relationship was observed between risk and percentile of tile scores for 0, 0.1th, 1st, 5th, 10th, and 25th percentiles whereas a negative relationship was observed for 50th, 75th, 90th, 99th, 99.9th, and 100th percentiles. The strong correlation between risk and individual tile score percentiles may explain the decent performance of some published algorithms such as maxpooling [ref] and meanpooling [ref]. In addition, the tile scores at individual percentiles may carry different information regarding the survival risk. Therefore, combining certain individual percentiles (such as MesoNet were

top/bottom 10 instances were used as prediction features) has been shown to provide better predictive performance. This may also explain the excellent performance for DeepDisMISL and illustrate the importance of utilizing the information of the entire distribution (i.e., combining multiple percentiles).

Figure 8 shows the representative tiles near the percentiles. It is interesting to notice that at lower percentiles (e.g., 0 – 75%), the tiles primarily included tumor cells. On the other hand, at the higher percentiles (e.g., 90%, 95, 99%, 99.9%, 100%), muscle appears to be the predominant tissue type. This may partly explain why at lower percentiles, there appears to be positive relationship between risk and the tile scores, whereas a reversed, negative relationship between risk and tile scores was observed at higher percentiles (Figure 7). It is intuitive that the tumor patches are related to higher risk while normal muscle patches may represent lower risk. This suggests that our algorithm is well interpretable and can help to reveal the relationship between morphological phenotypes and patients' risk.

3.6 Attention aggregation

We attempted to use attention mechanism in addition to the percentile structure on multiple neighborhood instances i.e., we assigned the same weight to each percentile location [6]. However, the results in Table 1 shows that attention mechanism did not improve the predictive ability. The C-index on MCO with cross validation from the attention-based model was 0.627, while the C-index using external validation dataset TCGA was 0.566. It is worth

mentioning that due to large number of parameters required for attention-based models, overfitting may be a challenge and prevented further improving the prediction.

4. Discussion

Risk stratification for cancer patients is currently largely based on cancer staging, mutation/molecular subtyping, and clinical features. Recently, outcome prediction algorithms based on histopathology images using deep learning have been proposed to stratify patients [6, 7, 10-12, 14-16, 28]. Although different approaches have been proposed to develop the deep learning survival models, identification of the most predictive image patches is an attractive strategy and has been an active area of research. Courtiol et al. trained a deep learning model (MesoNet) to derive a risk score for each image patch and selected the highest and lowest 10 scoring patches for each patient [8]. Further examination of the highest and lowest scoring patches demonstrated that the identified image patches were highly interpretable i.e., the high-risk patches were mainly located in stroma regions [8], consistent with prior biological knowledge.

In this study, we proposed and investigated the hypothesis of, instead of the highest and lowest scoring patches, the distribution of the risk scores of each WSI carries more information about slide-level risk and provides better prediction performance for the instance-based MIL algorithms. By incrementally adding additional patch scores at different percentiles (e.g., 1st, 5th, 25th, 75th, 95th, and 99th percentiles) to the highest and lowest scoring patches, the predictive performance of survival prediction in colorectal cancer was improved drastically. The superior performance of the distribution-based approach in our

study indicates that the overall distribution of patch survival scores of a WSI may be more representative of the slide-level survival risk. In addition, we demonstrated that including multiple neighborhood patches around each percentile could further improve the model performance compared to using only a single patch at each percentile.

We also systematically compared our proposed algorithm with six existing models: MesoNet [20], DeepAttnMISL [6], Meanpooling, Maxpooling (Top 1 instance), Maxpooling (Top 10 instance) and MeanFeaturePool [19]. The proposed distribution based algorithm (DeepDisMISL) was not only superior to MesoNet based on the top and bottom scoring patches [8], but also outperformed other state-of-the-art approaches. The mean C-index of our proposed DeepDisMISL (0.647) was markedly higher than that of the most recently published, state-of-the-art algorithm, DeepAttnMISL (C-index = 0.606) for the MCO dataset [6]. Compared to MesoNet [20], DeepDisMISL provided 6.3% and 2.8% improvement of mean C-index in the 5-fold cross-validation and external validation, respectively.

It is worth noting that Couture et al. proposed an instance-level MIL model that used local features of selected small image regions of an image for prediction [29]. Then a quantile function was implemented to aggregate the predictions from smaller regions of the image into an image-level classification (e.g., histologic subtype, genetic subtype, etc). They demonstrated that the quantile function can provide more complete description of heterogeneity within the image and improve image-level classification [29]. We proposed a

bag-level model for time-to-event survival data with two convolution 1-D layers with ReLU activation to aggregate all local features of the same tile to the global feature. The selected percentiles (instances) of the global feature vector were then selected as the input features for the model prediction.

It is known that, without external validation, deep learning models are prone to a high risk of bias due to batch effects [30]. As such, we validated and compared our model to other state-of-the-art algorithms using not only 5-fold internal cross validation, but also externally on an independent TCGA dataset. Both validations showed that the proposed DeepDisMISL provided superior performance over all the baseline algorithms, indicative of the robustness of our findings. Further evaluation and applications of DeepDisMISL in other types of cancers and in different population of colorectal cancer patients is warranted.

5. Conclusion

We developed a novel distribution based multiple-instance survival learning algorithm (DeepDisMISL) and validated our hypothesis that the more information regarding the distribution of the patch scores within a WSI, the better prediction for the survival using datasets from CRC patients. Including multiple neighborhood instances around each selected distribution location (e.g., percentiles) could further improve the predictive performance of DeepDisMISL. In addition, when compared against the state-of-the art baseline algorithms, DeepDisMISL provided superior prediction performance, and more accurate risk stratification for overall survival on both MCO CRC and TCGA COAD-READ datasets.

DeepDisMISL is highly interpretable with ability to reveal the relationships and interdependencies between morphological phenotypes and patient's cancer survival risk.

Acknowledgements:

The research of Xingyu Li, Min Cen, and Hong Zhang are partially supported by National Natural Science Foundation of China (No. 11771096, 72091212), Anhui Center for Applied Mathematics, and Special Project of Strategic Leading Science and Technology of CAS (No. XDC08010100). Jitendra Jonnagaddala is funded by the Australian National Health and Medical Research Council (No. GNT1192469). Jitendra also acknowledges the funding support received through the Research Technology Services at UNSW Sydney, Google Cloud Research (award# GCP19980904) and NVIDIA Academic Hardware grant programs. We also would like to thank the SREDH Consortium's (www.sredhconsortium.org) Translational Cancer Bioinformatics working group for the assistance with the MCO dataset access.

Contributions:

X.S.X., X.L., and H.Z. contributed to design of the research; J.J., X.L., and X.S.X. contributed to data acquisition; X.L., X.S.X., and M.C. contributed to data analysis. X.L., X.S.X., J.J., and H.Z. contributed to data interpretation. X.L., X.S.X., J.J., and H.Z. wrote the manuscript; and all authors critically reviewed the manuscript and approved the final version.

Figure Legends

Figure 1. Pipelines for MesoNet and DeepDisMISL. In multiple instance learning, each data sample is a bag of instances, and the bag can be seen as one patient in our approach. We extract features of tiles from the raw whole slide images, calculate tile-level scores, then obtain percentile scores to predict patient-level risk.

Figure 2. Performance for models with different percentiles (single tile at each percentile) for MCO dataset (internal validation) and TCGA dataset (external testing). Black solid dots = mean C-index value from 5-fold cross-validation experiments; Red solid dots = individual C-index values; Error bar = standard deviation.

Figure 3. Effects of number of neighborhood tiles at each percentile on model performance for MCO dataset (internal validation) and TCGA dataset (external testing). Solid line = smoothing curve; shaded area = standard deviation around the smoothing line; Black solid dots = mean C-index value from 5-fold cross-validation experiments; Red solid dots = individual C-index values; Error bar = standard deviation.

Figure 4 Comparison of different baseline algorithms using MCO dataset (internal validation) and TCGA dataset (external testing).

Figure 5. Kaplan-Meier plots comparing different algorithms using MCO dataset (internal validation) and TCGA dataset (external testing). For each algorithm, the median risk score in the training set was calculated and then applied as a threshold to stratify each patient into high-risk or low-risk group.

Figure 6: Distributions of tile scores. Patients are stratified into 10 different risk groups.

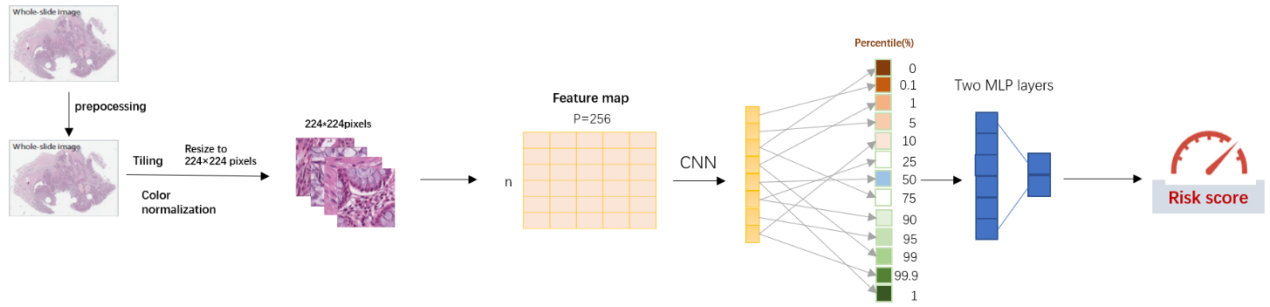
Figure 7: Relationship between the average tile score at each percentile and the risk. Patients are stratified into 10 different risk groups.

Figure 8: Visualization the spatial locations and morphologic features of tiles near different percentiles in a whole slide image. 13 different colors represent 13 percentile locations. 3

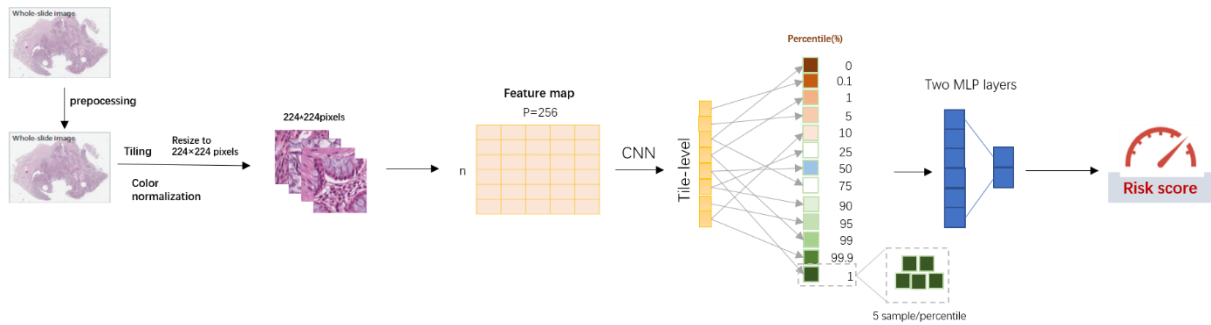
neighborhood tiles at each percentile are selected for visualization, and the tissue type of each tile are predicted by a published CRC tissue classifier.

Figure 1 (Pipeline)

(a) DeepDisMISL with single instance at each percentile



(b) DeepDisMISL with multiple instances at each percentile:



(c)

DeepDisMISL with only top and bottom instances:

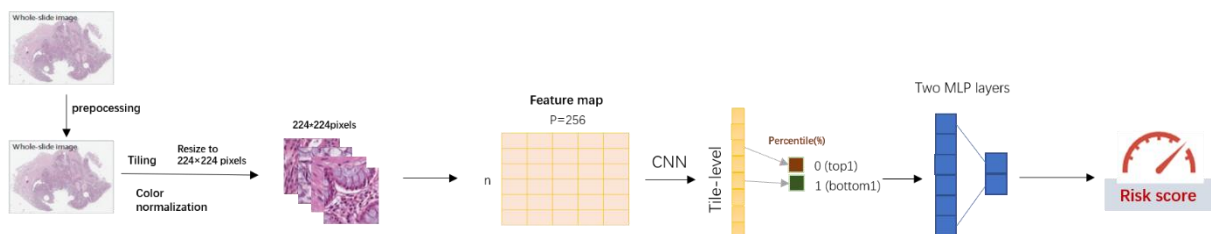


Figure 2:

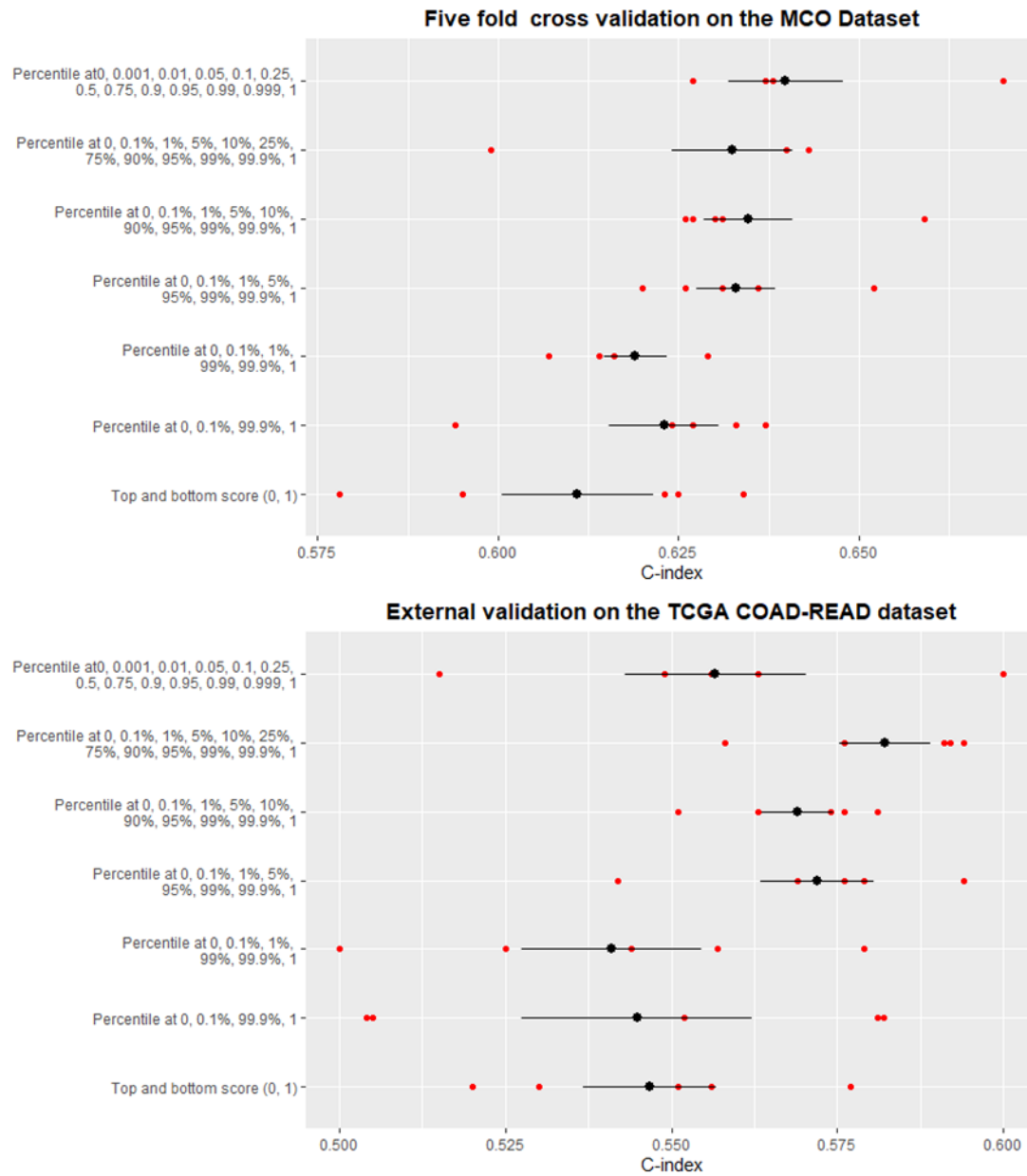


Figure 3:

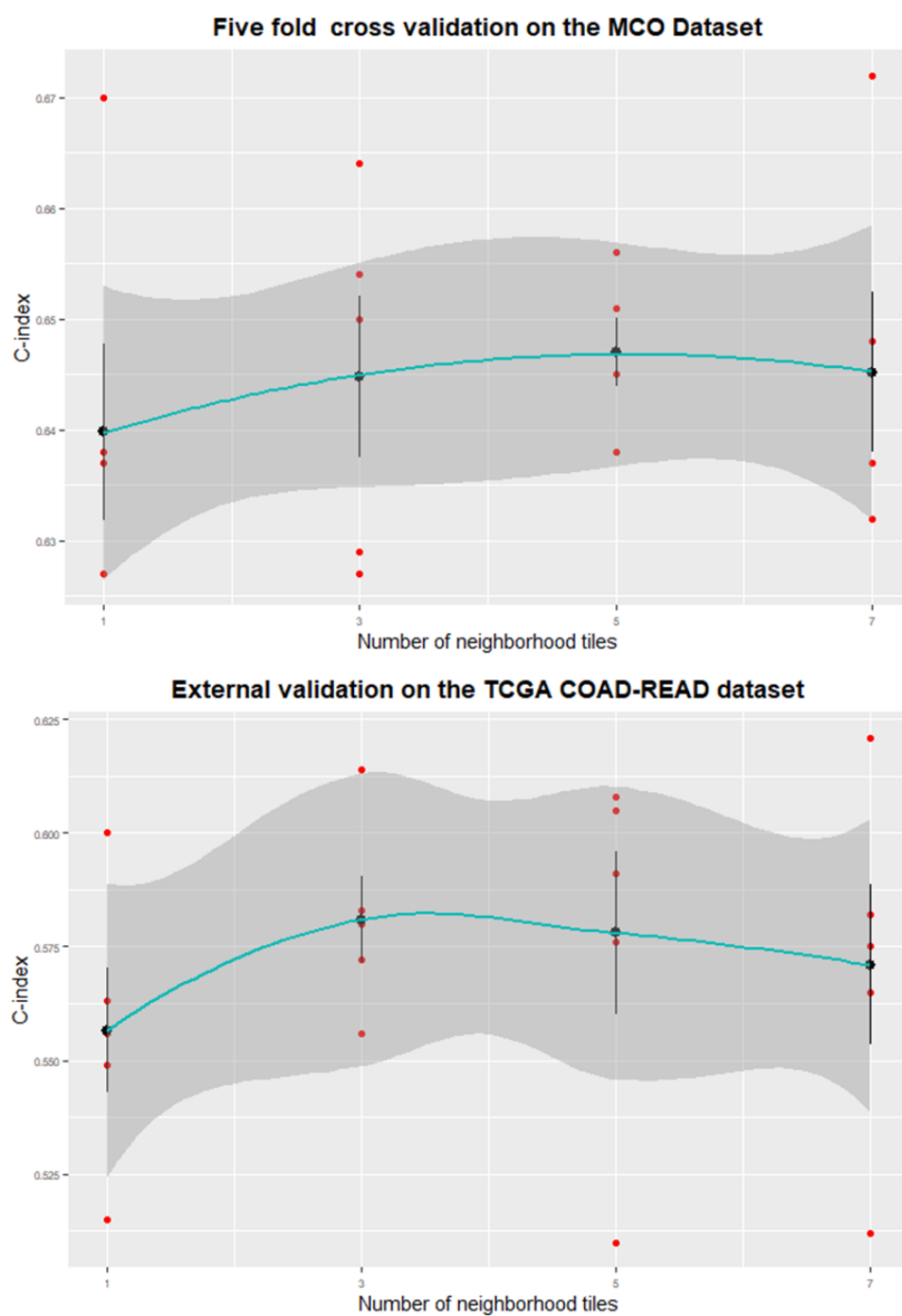


Figure 4:

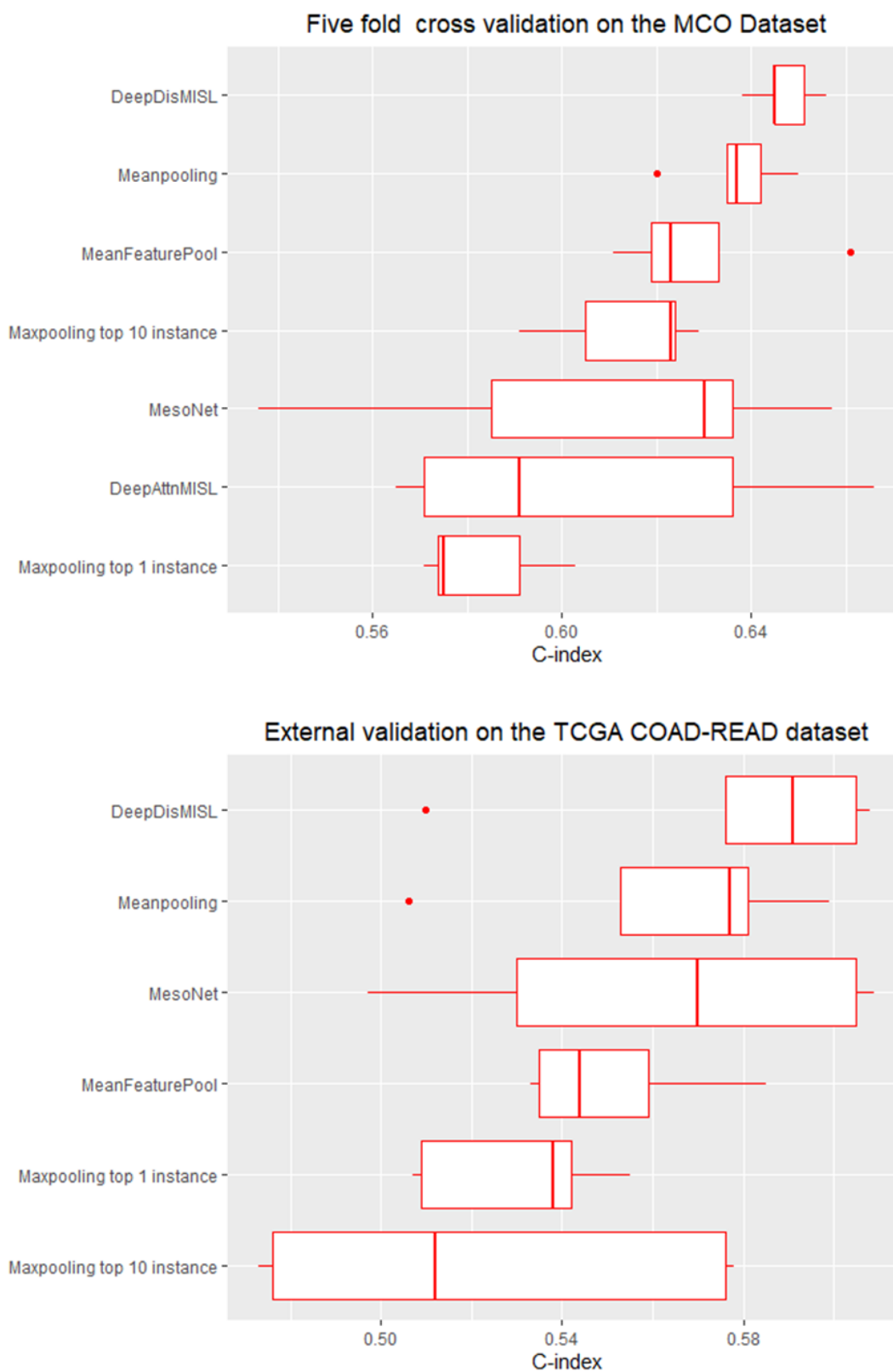
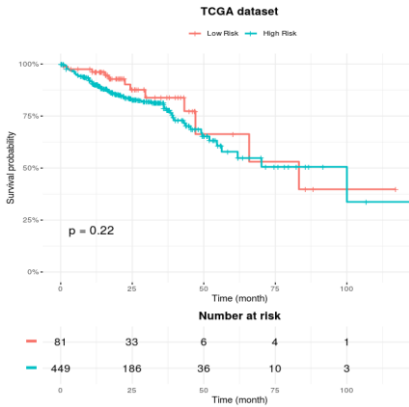
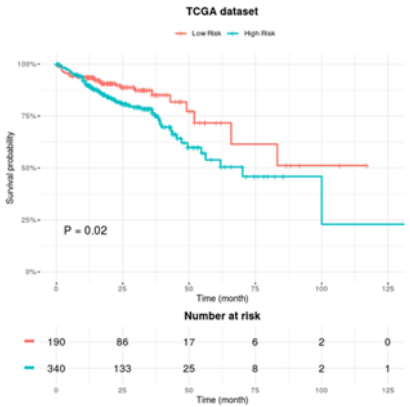
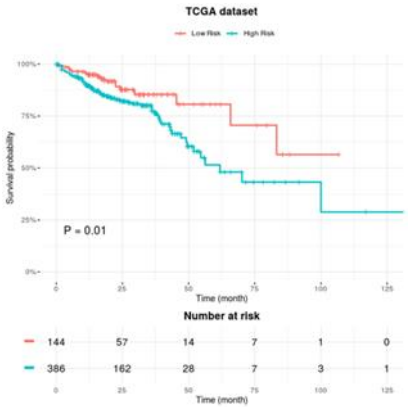
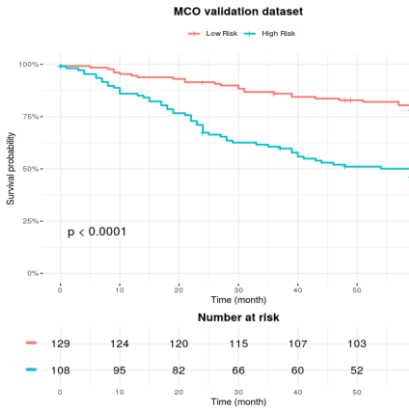
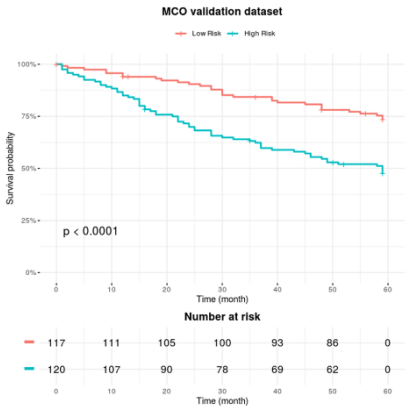
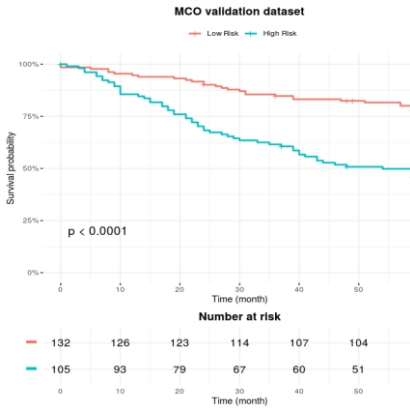


Figure 5:

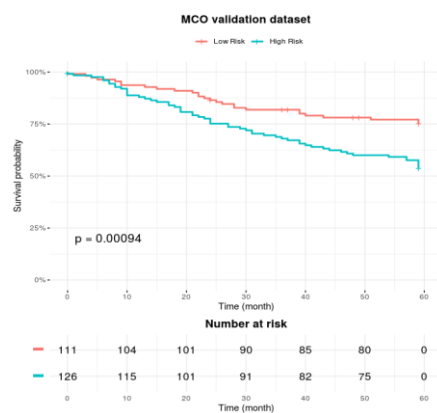
DeepDisMISL

MesoNet

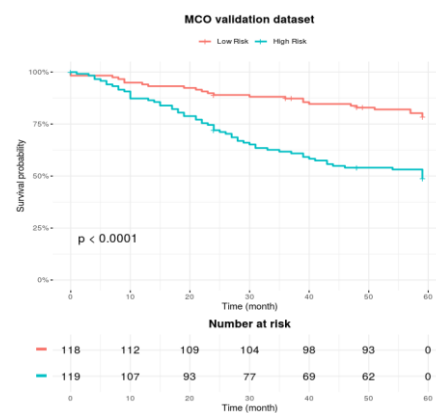
Meanpooling



Top 1 instance



Top 10 instance



MeanFeaturePool

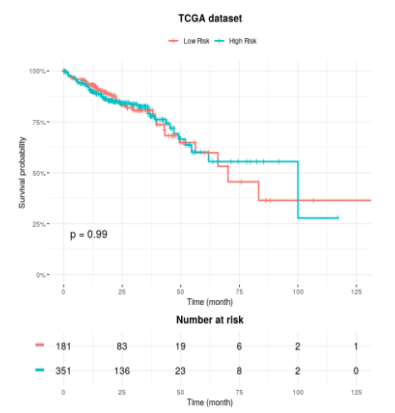
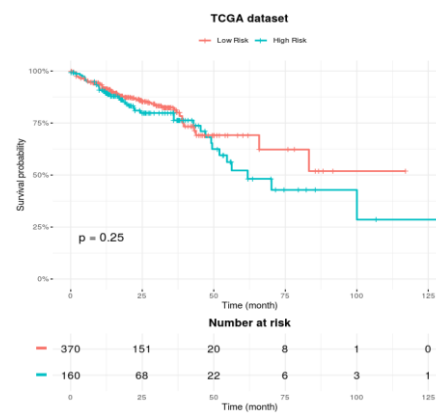
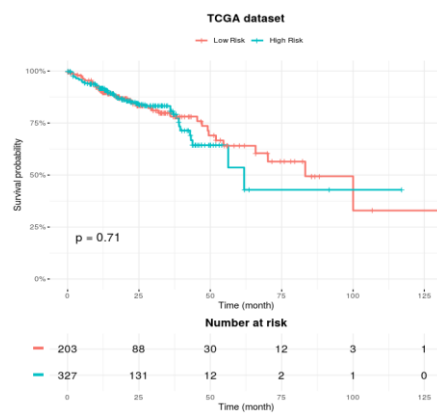
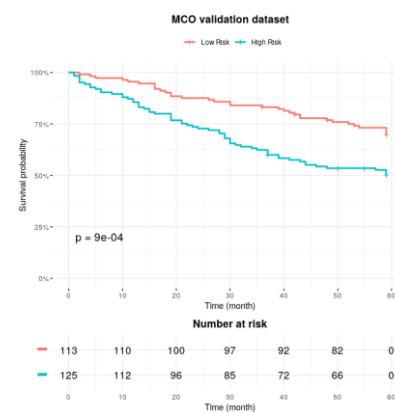
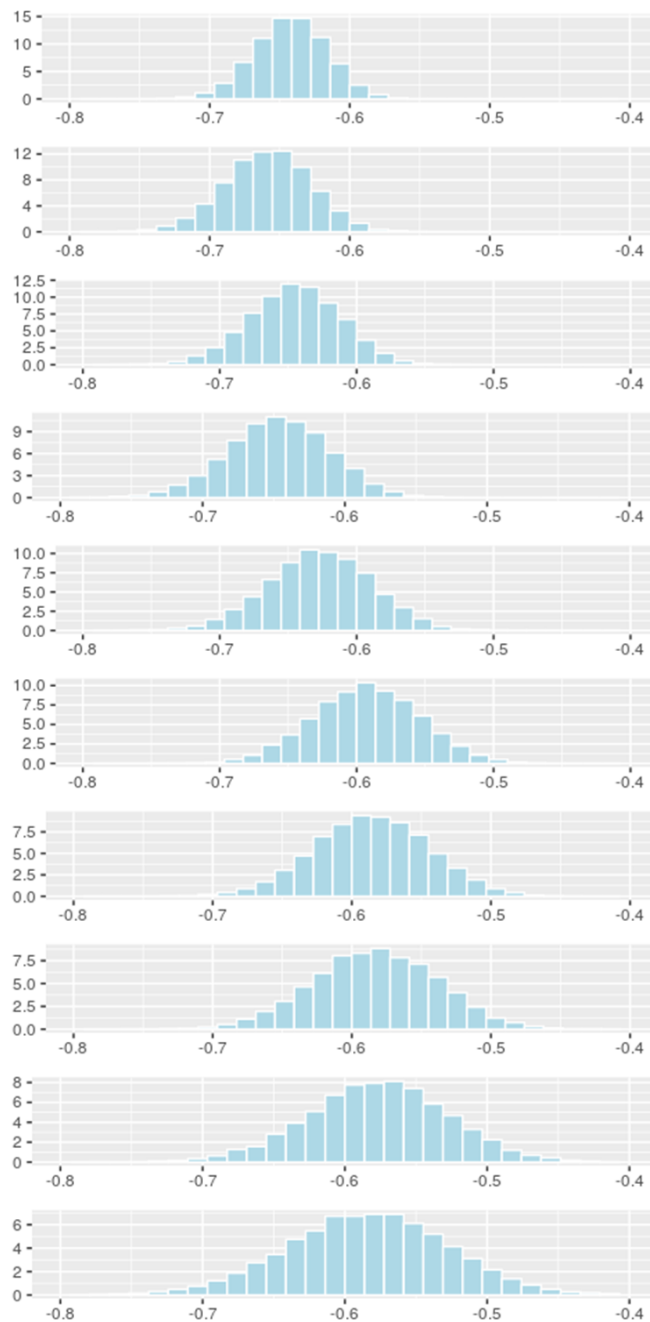


Figure 6:



Risk Group 10

Risk Group 9

Risk Group 9

Risk Group 7

Risk Group 6

Risk Group 5

Risk Group 4

Risk Group 3

Risk Group 2

Risk Group 1

Figure 7:

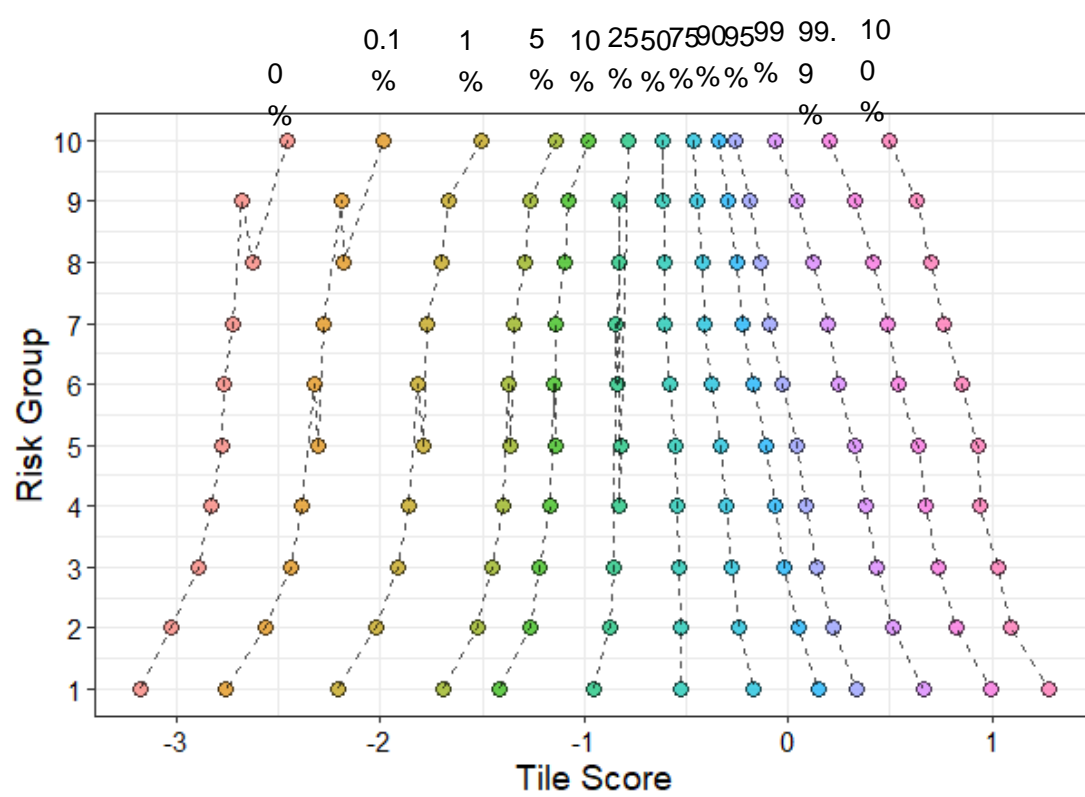
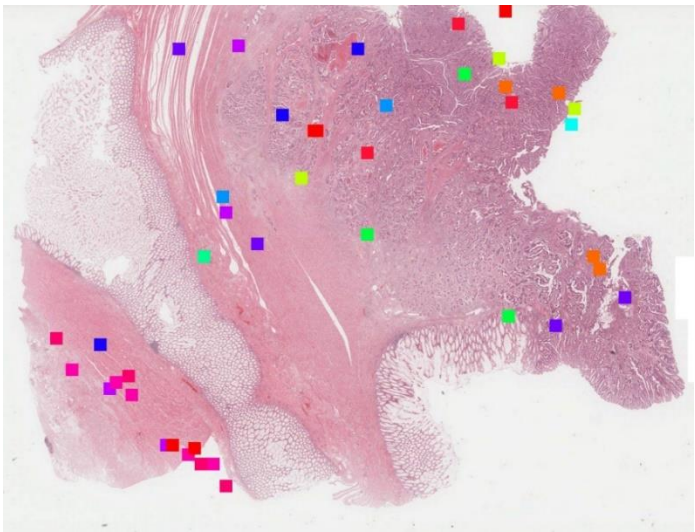


Figure 8:



0	STR	TUM	TUM	0.1%	STR	TUM	TUM
1%	TUM	TUM	TUM	5%	STR	ADI	TUM
10%	NORM	MUS	STR	25%	TUM	TUM	TUM
50%	STR	TUM	TUM	75%	TUM	TUM	TUM
90%	MUS	MUS	MUS	95%	MUS	MUS	MUS
99%	MUS	MUS	MUS	99.9%	MUS	MUS	MUS
100%	STR	STR	TUM				

Table 1. Performance of attention mechanism and no attention mechanism.

MCO CRC dataset - Internal Validation					
	Fold 1	Fold 2	Fold 3	Fold 4	Fold 5
No attention mechanism	0.66	0.64	0.65	0.65	0.65
With attention mechanism	0.67	0.65	0.62	0.61	0.6
TCGA COAD-READ dataset - External Validation					
No attention mechanism	0.61	0.58	0.61	0.51	0.59
With attention mechanism	0.55	0.58	0.6	0.56	0.54

Table 2: The structure of the DeepDisMISL

m_i : the number of percentile points O_i : risk score

Layer	Input	Output size
1D convolution layer	12000×256	12000×128
1D convolution layer	12000×128	$12000 \times 1(\text{score})$
Aggregating layer	12000×1	$m_i \times 1$
Fully-Con.	$m_i \times 1$	128×1
Fully-Con.	128×1	1 (O_i)

References:

1. Preisser, F., et al., *Intermediate-risk Prostate Cancer: Stratification and Management*. Eur Urol Oncol, 2020. **3**(3): p. 270-280.
2. Yu, F., et al., *Breast cancer prognosis signature: linking risk stratification to disease subtypes*. Brief Bioinform, 2019. **20**(6): p. 2130-2140.
3. Clifford, G.M. and C.J. Alberts, *Molecular Risk Stratification for Anal Cancer Prevention*. Clin Infect Dis, 2021. **72**(12): p. 2164-2166.
4. Rakha, E.A., et al., *Breast cancer prognostic classification in the molecular era: the role of histological grade*. Breast Cancer Res, 2010. **12**(4): p. 207.
5. Lu, M.Y., et al., *Data-efficient and weakly supervised computational pathology on whole-slide images*. Nat Biomed Eng, 2021. **5**(6): p. 555-570.
6. Yao, J., et al., *Whole slide images based cancer survival prediction using attention guided deep multiple instance learning networks*. Med Image Anal, 2020. **65**: p. 101789.
7. Zhu, X., et al. *WSISA: Making Survival Prediction from Whole Slide Histopathological Images*. in *2017 IEEE Conference on Computer Vision and Pattern Recognition (CVPR)*. 2017.
8. Courtiol, P., et al., *Deep learning-based classification of mesothelioma improves prediction of patient outcome*. Nature Medicine, 2019. **25**(10): p. 1519-1525.
9. Dietterich, T.G., R.H. Lathrop, and T. Lozano-Pérez, *Solving the multiple instance problem with axis-parallel rectangles*. Artificial Intelligence, 1997. **89**(1): p. 31-71.
10. Wulczyn, E., et al., *Interpretable survival prediction for colorectal cancer using deep learning*. NPJ Digit Med, 2021. **4**(1): p. 71.
11. Kather, J., et al., *Predicting survival from colorectal cancer histology slides using deep learning: A retrospective multicenter study*. PLoS Medicine, 2019. **16**: p. e1002730.
12. Wang, X., et al., *Prediction of BRCA Gene Mutation in Breast Cancer Based on Deep Learning and Histopathology Images*. Front Genet, 2021. **12**: p. 661109.
13. Bhargava, H.K., et al., *Computationally Derived Image Signature of Stromal Morphology Is Prognostic of Prostate Cancer Recurrence Following Prostatectomy in African American Patients*. Clin Cancer Res, 2020. **26**(8): p. 1915-1923.
14. Yamashita, R., et al., *Deep learning model for the prediction of microsatellite instability in colorectal cancer: a diagnostic study*. Lancet Oncol, 2021. **22**(1): p. 132-141.
15. Klimov, S., et al., *Predicting Metastasis Risk in Pancreatic Neuroendocrine Tumors Using Deep Learning Image Analysis*. Front Oncol, 2020. **10**: p. 593211.
16. Chen, P., et al. *Hierarchical Phenotyping and Graph Modeling of Spatial Architecture in Lymphoid Neoplasms*. 2021. arXiv:2106.16174.
17. Naderi Parizi, S., et al. *Automatic Discovery and Optimization of Parts for Image Classification*. 2014. arXiv:1412.6598.
18. Courtiol, P., et al. *Classification and Disease Localization in Histopathology Using Only Global Labels: A Weakly-Supervised Approach*. 2018. arXiv:1802.02212.
19. Durand, T., N. Thome, and M. Cord. *WELDON: Weakly Supervised Learning of Deep Convolutional Neural Networks*. in *2016 IEEE Conference on Computer Vision and Pattern Recognition (CVPR)*. 2016.

20. Courtiol, P., et al., *Deep learning-based classification of mesothelioma improves prediction of patient outcome*. Nat Med, 2019. **25**(10): p. 1519-1525.
21. Jonnagaddala, J., et al., *Integration and Analysis of Heterogeneous Colorectal Cancer Data for Translational Research*. Stud Health Technol Inform, 2016. **225**: p. 387-91.
22. Ward, R. and N. Hawkins, *Molecular and Cellular Oncology (MCO) study whole slide image collection*, <http://dx.doi.org/10.4225/53/555921d09f76b>, UNSW, Editor. 2015.
23. Bonneville, R., et al., *Landscape of Microsatellite Instability Across 39 Cancer Types*. JCO Precis Oncol, 2017. **2017**.
24. Otsu, N., *A threshold selection method from gray level histograms*. IEEE Transactions on Systems, Man, and Cybernetics, 1979. **9**: p. 62-66.
25. Li, X., et al. *Improving Feature Extraction from Histopathological Images Through A Fine-tuning ImageNet Model*. 2022. arXiv:2201.00636.
26. Tibshirani, R., *The lasso method for variable selection in the Cox model*. Stat Med, 1997. **16**(4): p. 385-95.
27. Li, X., et al., *A retrospective analysis using deep-learning models for prediction of survival outcome and benefit of adjuvant chemotherapy in stage II/III colorectal cancer*. J Cancer Res Clin Oncol, 2022.
28. Muhammad, H., et al. *EPIC-Survival: End-to-end Part Inferred Clustering for Survival Analysis, Featuring Prognostic Stratification Boosting*. 2021. arXiv:2101.11085.
29. Couture, H.D., et al. *Multiple Instance Learning for Heterogeneous Images: Training a CNN for Histopathology*. 2018. arXiv:1806.05083.
30. Howard, F.M., et al., *The Impact of Digital Histopathology Batch Effect on Deep Learning Model Accuracy and Bias*. bioRxiv, 2020: p. 2020.12.03.410845.